Biomolecular interactions of 1,3-bis(2-arylimino)isoindolate-based palladium(II) complexes: Substitution kinetics, DNA/protein-binding, and molecular docking approaches

Daniel O. Onunga [a,b,*], Reinner O. Omondi [a,g], Meshack Sitati [a,c], Gershom K. Mutua [a,d], Deogratius Jaganyi [e,f], Allen Mambanda [a]

[a] School of Chemistry and Physics, University of KwaZulu-Natal, Private Bag X01, Scottsville, Pietermaritzburg 3209, South Africa
[b] Department of Chemistry, Maseno University, P. O. Box 333-40105, Maseno, Kenya
[c] Department of Mathematics and Physical Sciences, Maasai Mara University, P.O. Box 861 Narok 20500, Kenya
[d] Department of Pure and Applied Chemistry, Masinde Muliro University of Science and Technology, P.O. Box 190, Kakamega 50100, Kenya
[e] School of Pure and Applied Sciences, Mount Kenya University, P.O. Box 342-01000, Thika, Kenya
[f] Department of Chemistry, Durban University of Technology, P.O. Box 1334, Durban 4000, South Africa
[g] Department of Chemistry, University of Cape Town, Rondebosch 7701, South Africa

ARTICLE INFO

ABSTRACT

A series of 1,3-bis(2-arylimino)isoindoline Pd(II) complexes core *viz.;* Chlorido(1,3-bis(2-pyridylimino) isoindoline)palladium(II), **Pd1**, Chlorido(1,3-bis(4-methyl-2-pyridylimino)isoindoline)palladium(II), **Pd2**, Chlorido(1,3-bis(2-pyridylimino)benz(*f*)isoindoline)palladium(II), **Pd3** and Chlorido(1,3-Bis(1-isoquinolylimino)isoindoline)palladium(II), **Pd4** were synthesized, appropriately characterized and the crystal structure of **Pd2** elucidated. The kinetics and mechanism of the substitution of the chloride ligand with thiourea ligands, **Tu**, **Dmtu** and **Tmtu**, from the complexes were investigated under *pseudo*-first-order conditions. The analyses were performed using stopped-flow analyzer or UV–visible spectrophotometer. The reactions proceeded through two consecutive steps for most complexes with exception of **Pd4** showing only a single step. The substitution rates followed the order: **Pd1**>**Pd2**>**Pd3**>**Pd4** due to varying degrees of steric influences and σ-/π-donations caused by the methylation and benzannulation on the *cis-/trans*-positions of the pyridyl rings of the BPI. The quenching of the fluorescence of CT-DNA/EB by the Pd(II) complexes suggests static quenching mechanism. The simulated docking of the complexes onto CT-DNA suggests they bind mainly in the minor grooves of DNA. The UV–Visible absorption titrations and quenching of tryptophan (Trp) fluorescence of BSA by the complexes depict reasonable interactions which occur mainly in the hydrophobic domains of the former. The order of strength of the interaction of the complexes with DNA or BSA is consistent with the rates of substitution kinetics.

1. Introduction

Designing less toxic antitumour-active Pd(II) drugs remains a challenge because their rates of ligand exchange are 10^2–10^5 times higher than their analogous Pt(II) compounds.[1] To reduce the toxicity associated with highly reactive Pd(II) complexes towards biological nucleophiles, strong σ-/π-donor NˆNˆN chelators with a measurable steric hindrance at the lateral positions are needed in the design of Pd(II) drug candidates that are moderately inert towards substitution. Such structural modifications of the non-leaving ligand can slow down the rate of

substitution and thus stabilize the complexes against deactivation by biological nucleophiles. This can ensure better prospects of the Pd(II) complexes reaching and ultimately interacting with DNA, the target for their antitumour action.[2] At the same time, side reactions that manifest toxicity are also reduced.[3]

The 1,3-bis(2-pyridylimino)isoindolines (BPIs) are one such class of strong σ-/π-donor NˆNˆN chelators that can potentially bring moderate inertness to their Pd(II) complexes. BPIs are pincer-type tridentates, whose chemistry has attracted great interest from the time they were discovered in the 1950 s due to their special coordination.[4] BPIs

coordinate as monoanionic tridentates (NˆNˆN) to form octahedral and square-planar complexes with most metal ions in the transition group such as Ru(II/III), Pt(II) and Pd(II)[5] among others.[5b,6] Most of these complexes bear twin and flexible six-membered chelates around the d^8 metal ions and have near-perfect bite angles. Some of the complexes have found applications in catalysis[7] electrochemical and photo-physical applications [5c,8]. However, there are no literature reports on their biomedical applications. In particular, their anti-tumour activity is unreported, yet some of the free BPI ligands have been reported to have anticancer activity.[9] Literature data on substitutional lability of Pt (BPIs) complexes is still scanty.[10] Therefore, studying the rates of ligand substitution from these complexes could be very insightful in designing and discovering BPI-ligated Pt(II)/Pd(II) complexes with antitumour potential.

From a coordination point of view, terpyridyl or its conjugated derivatives make a good reference class of NˆNˆN chelators for forming stable Pd(II)/Pt(II) complexes. Unlike the Pd(II)/Pt(II)(BPIs) complexes, their terpyridyl analogues are rigid and form twin 5-membered chelates with notable acute bite angles. These complexes are highly reactive. Benzannulation of the core NˆNˆN of the ligand on different positions of the pyridyl rings can increase or lower the substitution rate, in keeping with the respective position. For example, when one or both lateral pyridyl rings of the ligand, NˆNˆN, is/are changed to a deprotonated phenyl group (a strong σ-donor *cis* to the labile ligand), the rate of substitution is reduced.[11] However, the rate is increased when the strong σ-donor phenyl ring is positioned *trans* to the labile ligand group due to the ground state *trans*-labilizing effect.[12] Furthermore, when terpyridine ligand is extended by π-conjugation through the incorporation of an additional ring to increase the π-surfaces, reactivity is also increased due to charge dissipation through π-back bonding from the metal's dπ-orbitals into the π*-orbitals of the NˆNˆN ligand.[12–13] However, benzannulation *via* the *cis* positions lowers the substitution rate because of the poor π-acceptability characteristics of the benzo-pyridines compared to pyridines.[14].

Notably, the incorporation of methylene bridging groups,[1b,15] for example between the terpyridyl results in a flexible and steric imposing tri(pyridyl)dimethane (tpdm)[15a] ligand also known to form six-membered chelates around the central metal atom just like the BPIs. By comparing the substitution rate constants in several related Pd(II) complexes,[16] it was demonstrated that the rates could reduce by up to six orders of magnitude[15a] due to steric-imposing effects. On the other hand, comparative retardation factors for the analogous Pt(II) complexes were lower by a small factor of about 10.[15b].

Other studies that explored the reactivity of several NˆNˆN chelated Pt(II) complexes when the ligands formed six-membered flexible chelates incorporating azaindole units,[1a,15a,17] also reported a similar decrease in the substitution rates in comparison to the reference complex, Pt(II)(terpy)Cl]$^+$.[17b,d] A combination of an out-of-plane steric effect due to the relatively flexible ligands and a strong π-donation of the pyrollic-N of the azaindoles at the *cis* positions synergistically lowered the rate of substitution. In another study, the substitution rates from [Pt (II)(1,3-bis(2-pyridylimino)isoindolate)Cl]$^+$ and its analogues for which the π-conjugation of their non-leaving ligands was increased, were compared to that of Pt(II)(terpy)Cl]$^+$.[10] The former complexes were found to be relatively more inert. Also important in slowing the reactivity of the derivatives relative to the reference Pt(II)(terpy)Cl]$^+$ complex, is the featuring of sterically bulky aromatic groups or site-shielding ancillary substituents at the lateral positions of the terpyridyl-based NˆNˆN ligand.[17b,c] These groups can effectively block the facile approach of the entering nucleophile towards the coordinated metal. This steric effect conferred by proximal groups onto the leaving group can dominate over electronic factors for the kinetic control of the substitution reaction.[18].

As a build-up to this knowledge, Pd(II) complexes coordinated with BPIs as flexible, six-membered core NˆNˆN ligands (shown in Fig. 1) were synthesized and kinetically studied using bio-relevant thiourea nucleophiles to establish their structure–reactivity relationships. Thiourea nucleophiles were chosen due to their exemplary high aqueous solubility, different nucleophilicity, variable steric hindrances, neutral donor character, binding properties as well as their biological relevance. [19] Moreover, sulfur-donor nucleophile exhibit the combined properties of thioethers (π-donor and σ-acceptor) and thiolates (σ-donor) in their substitution reactions.[19a,20].

The structures of the BPIs were varied through, the addition of the methyl groups at the 4,4′-positions of the *cis*-pyridyl coordinated units, or through benzannulation either at the isoindolate head (*trans* to leaving group) or at the bis(pyridyl) rings (*cis* positions to the leaving group). Density function theory (DFT) calculations were done to provide more information to help understand the trends observed in the rates of substitution. The biomolecular titrations of the complexes were probed to determine their mode of action (i.e. groove binding, intercalation, or covalent binding) with the target, thymus DNA (CT-DNA). Additionally, we evaluated the protein binding properties of the complexes to asses their ease of transportation, distribution and metabolism in the plasma.

2. Experimental

2.1. Materials and methods

Syntheses were done using standard Schlenk techniques in the presence of nitrogen atmosphere. 1,2-dicyanobenzene, 1,3-diiminobenz (f)isoindoline, 1-butanol, triethylamine (NEt₃), 2-amino-4-methylpyri-dine, 2-aminopyridine, 1-aminoisoquinoline, anhydrous 1-butanol, thiourea nucleophiles, and benzene were purchased from Aldrich. Dichloro(1,5-cyclooctadiene)palladium(II) [Pd(COD)Cl₂, 99%], anhydrous calcium chloride (CaCl₂), and Bis(benzonitrile)dichloropalladium

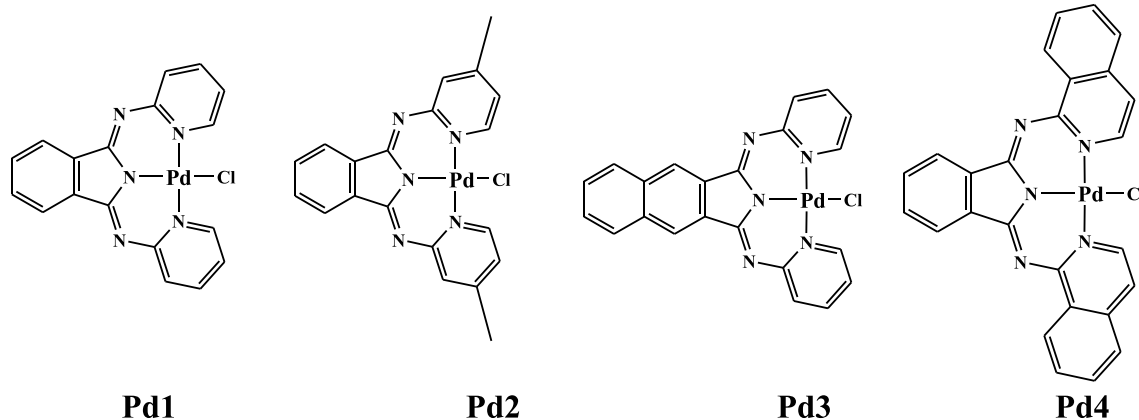**Pd1**　　　　**Pd2**　　　　**Pd3**　　　　**Pd4**

Fig. 1. Structures of the Pd(II) complexes studied.

(II), $(C_6H_5CN)_2PdCl_2$, 95% were used as received from Sigma-Aldrich.

2.2. Ligands syntheses

The ligands, 1,3-bis(2-pyridylimino)isoindoline, **L1**, and 1,3-bis(4-methyl-2-pyridylimino)isoindoline, **L2**, [21] 1,3-bis(2-pyridylimino) benz(f)isoindoline, **L3**, [6a] and 1,3-bis(1-isoquinolylimino)isoindoline, **L4**, [5c,22] were synthesized following standard literature procedures. The details of their synthetic procedures and characterization are given as notes, NSI 1, in the Electronic Supplementary Information (ESI‡).

2.3. Synthesis of complexes

The Pd(II) complexes; **Pd1**, **Pd2**, **Pd3** and **Pd4** were synthesized following published procedures.[5b, 5c, 5e, 7].

2.3.1. Chlorido(1,3-Bis(2-pyridylimino)isoindoline)palladium(II), Pd1

Pd(COD)Cl$_2$ (142.8 mg, 0.5 mmol) was added into a stirring solution of **L1** ligand, 1,3-bis(2-pyridylimino)isoindoline (149.5 mg, 0.5 mmol) in methanol (20 mL) and triethylamine, NEt$_3$ (70 µL, 0.5 mmol) added. The mixture was heated to 50 °C under nitrogen atmosphere for 24 h. The mixture was cooled and the precipitate formed was filtered off. The water-leached solid was further purified by washing and the crude product obtained was recrystallized from dichloromethane/n-hexane yielding a bright yellow solid. Yield: 110 mg (50 %). ^{1}H NMR (400 MHz, CDCl$_3$, ppm) $\delta = 9.88$ (m, 2H), 8.06 (m, 2H), 7.86 (m, 2H), 7.63 (m, 4H), 7.09 (m, 2H). ^{13}C NMR (100 MHz, CDCl$_3$, ppm) $\delta = 153.9, 152.3, 120.0, 122.6, 126.7, 131.7, 138.0, 138.4, 139.5$. TOF-MS ESI$^+$ $m/z = 461.9970$ (M + Na)$^+$. *Anal. Calc. for* C$_{18}$H$_{12}$N$_5$PdCl: C, 49.11; H, 2.75; N, 15.91. *Found:* C, 48.72; H, 2.39; N, 15.92.

2.3.2. Chlorido(1,3-Bis(4-methyl-2-pyridylimino)isoindoline)palladium (II), Pd2

To a mixture of Pd(PhCN)$_2$Cl$_2$ (767.1 mg, 2.0 mmol) and **L2** ligand, 1,3-bis(4-methyl-2-pyridylimino)isoindoline (654 mg, 2.0 mmol) in benzene (20 mL), triethylamine, NEt$_3$ (279 µL, 2.0 mmol) was added. The mixture was then stirred at room temperature under a nitrogen atmosphere for 2 days. The precipitate product observed was separated by filtration. The solid was washed three times with water (50 mL) and thereafter recrystallised from a dichloromethane/n-hexane solution mixture yielding a yellow-ochre solid. Single crystals of **Pd2** of good quality for X-ray diffraction analysis were obtained via recrystallization from slow evaporation of its chloroform solution. Yield: 150.8 mg (16.1 %). ^{1}H NMR (400 MHz, CDCl$_3$, ppm): $\delta = 9.70$ (d, 2H), 8.02 (m, 2H), 7.61 (m, 2H), 7.42 (s, 2H), 670 (m, 2H), 2.42 (s, 6H). ^{13}C NMR (100 MHz, CDCl$_3$, ppm) $\delta = 153.1, 152.1, 151.6, 149.4, 138.1, 131.6, 126.9, 122.4, 121.5, 20.9$. TOF-MS ESI$^+$ $m/z = 469.9752$ (M + H)$^+$. *Anal. Calc. for* C$_{20}$H$_{16}$N$_5$PdCl: C, 51.30; H, 3.44; N, 14.96. *Found:* C, 51.33; H, 3.11; N, 15.29.

2.3.3. Chlorido(1,3-Bis(2-pyridylimino)benz(f)isoindoline)palladium(II), Pd3

To a mixture of Pd(COD)Cl$_2$ (142.8 mg, 0.5 mmol) and ligand **L3**, 1,3-bis(2-pyridylimino)benz(f)isoindoline (174.5 mg, 0.5 mmol) in methanol (20 mL), triethylamine, NEt$_3$ (70 µL, 0.5 mmol) was added. The mixture was then heated to 50 °C under a nitrogen atmosphere for 2 days. The mixture was left to cool to room temperature and the precipitated solid was separated by filtration. The solid was washed three times with water (50 mL) to remove impurities. The washed precipitate was recrystallised from a dichloromethane/n-hexane solution mixture yielding a yellow solid. Yield: 133.3 mg (54.4 %). ^{1}H NMR (400 MHz, CDCl$_3$, ppm) $\delta = 9.85$ (m, 2H), 8.50 (s, 2H), 8.05 (q, 2H), 7.85 (m, 2H), 7.64–7.59 (m, 4H), 7.06 (m, 2H). ^{13}C NMR (125 MHz, CDCl$_3$, ppm) $\delta = 153.9, 153.6, 152.3, 139.3, 131.1, 134.0, 130.0, 128.0, 126.5, 123.0, 119.6$. TOF-MS ESI$^+$ $m/z = 954.9501$ (2 M + Na)$^+$. *Anal. Calc. for* C$_{22}$H$_{14}$N$_5$PdCl: C, 53.90; H, 2.88; N, 14.29. *Found:* C, 53.78; H, 2.76; N,

13.99.

2.3.4. Chlorido(1,3-Bis(1-isoquinolylimino)isoindoline)palladium(II), Pd4

To a mixture of Pd(COD)Cl$_2$ (142.8 mg, 0.5 mmol) and ligand **L4**, 1,3-bis(1-isoquinolylimino)isoindoline (199.5 mg, 0.5 mmol) in methanol (20 mL), triethylamine, NEt$_3$ (70 µL, 0.5 mmol) was added. The mixture was stirred at 50 °C under a nitrogen atmosphere for 2 days. The mixture was left to cool to room temperature and the precipitated solid was separated by filtration. The solid was washed three times with water (50 mL) to remove impurities. The washed precipitate was recrystallised from a dichloromethane/n-hexane solution mixture yielding an orange solid. Yield: 98.7 mg (36.5 %). ^{1}H NMR (400 MHz, CDCl$_3$, ppm) $\delta = 9.74$ (d, 2H), 9.32 (d, 2H), 8.29 (q, 2H), 7.84 (d, 2H), 7. 83 (d, 2H), 7.76—7.72 (m, 4H), 7.41 (d, 2H). ^{13}C NMR (125 MHz, CDCl$_3$, ppm) $\delta = 151.0, 145.4, 138.4, 137.1, 132.5, 131.8, 128.4, 128.2, 127.9, 126.9, 122.9, 118.1$. TOF-MS ESI$^+$ $m/z = 855.3387$ (M + 4DMSO + 3H)$^+$. *Anal. Calc. for* C$_{26}$H$_{16}$N$_5$PdCl: C, 57.80; H, 2.98; N, 12.96. *Found:* C, 57.51; H, 2.66; N, 12.93.

2.4. Instrumentation and physical measurements

^{1}H and ^{13}C NMR spectra were obtained from either a Bruker Avance DPX 400 or a DPX 500 NMR with a 5 mm BBOZ probe at 30 °C. A Waters TOF Micro-mass LCT Premier or a Shimadzu LC-MS 2020 spectrophotometer fitted with an electron spray ionization in the positive mode (ESI$^+$) was used for mass spectroscopic analysis. The respective mass and NMR spectra for the complexes and ligands are shown in Figures SI 1–21, ESI‡. For elemental analysis of the ligands and complexes, a Carlo Erba Elemental Analyzer 1106 was used while the single-crystal X-ray structure of **Pd2** was solved on a Bruker Apex Duo fitted with an Incoatec microsource operating at 30 W power and an Oxford Instruments Cryojet operating at 100(2) K. A Cary 100 Bio UV–visible spectrophotometer was used for pre-determination of suitable wavelengths which were used for monitoring each substitution reactions and measuring the rate constants for slower reactions. An Applied Photophysics SX 20 stopped-flow reaction analyzer coupled to an online data acquisition system was used for quantifying fast reaction rate constants. The instrument was thermo-controlled within ± 0.1 °C.

2.5. X-ray crystallography

A suitable crystal (0.34 × 0.22 × 0.14) mm^3 was selected and mounted on a MITIGEN holder in paratone oil on a Bruker APEX-II CCD diffractometer. The crystal was kept at $T = 100(2)$ K during data collection. Using Olex2,[23] the structure was solved with the ShelXS-2013[24] structure solution program, using the direct solution method. The model was refined with version 2016/6 of ShelXL[25] using Least Squares minimization. The crystal structure was deposited (CCDC number 1829125) at Cambridge Crystallographic Data Centre.

2.6. Computational analysis

The DFT minimum energy geometric structures were computed by the Gaussian 09 program suite[26] using the B3LYP (Becke 3-Lee-Yang-Parr) functional method,[27] utilizing the LANL2DZ (Los Alamos National Laboratory 2 Double ζ)[28] as the basis set. The influence of the solvent on the geometry of the complexes was evaluated in ethanol via the single-point computation using the conductor-like polarizable continuum model (C-PCM).[29] All the complexes were modelled as neutral metal compounds in their singlet state. The calculated geometric and electronic empirical data was correlated to the observed kinetic trends.

2.7. Kinetic analysis

The Pd(II) complexes were prepared by first dissolving accurately weighed amounts in a few drops of THF and then topped up to 100 mL

using water containing 10 mM NaCl, to achieve a final concentration of 1.0×10^{-4} M. The solvent containing NaCl was used to prevent solvolysis since it does not easily coordinate to square planar d^8 ions.[30] Fresh solutions of the nucleophiles which were 50–10 folds more concentrated than each Pd(II) complex were made by dissolving weighed amounts of each nucleophile in the same solvent system as used for the complexes and were diluted accordingly. The excess concentration folds in each nucleophile over the complex were used to maintain *pseudo*-first-order reaction conditions.

Suitable wavelengths at which the kinetic reactions could be monitored were predetermined spectrophotometrically by recording the spectral changes between 800 nm and 200 nm for all reactions between each complex and the nucleophiles. The wavelengths at which each reaction was monitored are presented in Table SI 1, ESI‡. Reactions that were studied on the Stopped-flow analyzer (τ less than 16 min) were initiated by an automated mixing of equal volumes of the complex and ligand solutions directly into the stopped-flow reaction cell while those reactions run on the UV–visible absorption spectrophotometer were initiated through manual mixing of the thermally pre-equilibrated solutions in a tandem cuvette. The rate constants were measured under *pseudo*-first-order conditions as a function of each nucleophile concentration [Nu] at 25 °C as well as the temperature-dependent reactions in the range between 20 °C and 40 °C at 5 °C intervals.

2.8. DNA and protein binding experiments

2.8.1. UV–Visible absorption and fluorescence spectroscopy

The UV–Visible absorption titrations of CT-DNA and the quenching of the fluorescence of CT-DNA/ethidium bromide (EB) with the complexes were carried out according to the previously reported literature procedures.[1b,31].

2.9. Molecular docking details

Molecular docking of the complexes onto DNA or BSA was carried out using the AutoDock Vina software suite.[32] The crystal structures of DNA (PDB ID: 1Z3F) and BSA (PDB ID: 4F5S) were obtained from the protein data bank (http://www.rcsb.org/) at a resolution of 1.60 and 2.47 Å, respectively. The structures were refined by removing hetero atoms, solvent molecules (H₂O), and cofactors. Polar hydrogen atoms as well as Kollman charges were added to the structures. The Gasteiger charges were also computed for each atom, while non-polar hydrogens were merged into carbon atoms. The coordination spheres of the Pd(II) complexes were generated from DFT calculations, and the optimized geometry was converted to PDB format with the help of GaussView 5.0 software. The complexes and receptors were prepared using AutoDock Tools. In the post-docking analysis, the binding sites of the complexes were constrained to the entire receptor with a grid spacing of 0.375 Å. BIOVIA Discovery Studio Visualizer 2022 package was used to produce molecular animations, atomic interaction measurements, and structural images.

3. Results and discussion

3.1. X-ray analysis

The X-ray crystal structure for the **Pd2** ($C_{20}H_{16}ClN_5Pd$) complex is depicted in Fig. 2, while the crystallographic data, refinement structure parameters as well as selected bond lengths and angles of the complex are shown in Tables SI 2, and SI 3 in ESI‡, respectively.

In the crystal structure of **Pd2**, the Pd(II) metal ion is coordinated in a tridentate fashion to the N1, N3 and N5 atoms of the **L2** ligand at distances of 2.057(6), 1.964(1) and 2.061(2) Å, respectively. The fourth coordination site is occupied by the chloride atom at a bonding distance of 2.339(1) Å. These bond lengths are within the range observed for other [Pd(II),(BPI)Cl]⁺ complexes.[5b,5e,7,33] The central Pd–N3 bond
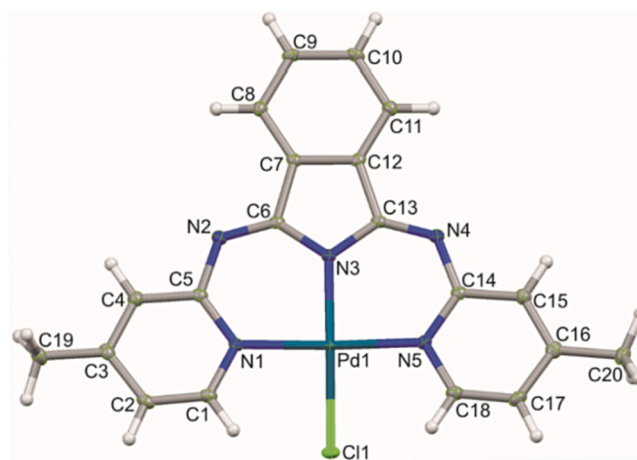

Fig. 2. The structure of Pd2 showing the atom numbering scheme. The displacement ellipsoids of atoms are shown at the 50% probability level.

distance is noticeably shorter than the other two Pd–N bond lengths. This is attributed to the increased ionic nature of the bond [7] because of the largely localized negative charge at the N3.[34].

The coordination geometry of the **Pd2** complex adopts almost a perfect square-planar. However, the Pd–Cl bond is slightly displaced from the PdN1N3N5 plane. The bite angle (N1–Pd–N5) of the ligand is 172.17(6)°, which is a slight deviation from linearity (180°). This is as expected of the six-membered flexible chelates of the [Pt/Pd(II)(BPI)X]⁺ complexes. However, the angle N3–Pd–Cl1, is markedly non-linear at 165.27(5)° and is attributed to the repulsive interactions between the *ortho*-hydrogen atoms of the pyridyl groups and the coordinated chloride atom.[7] These bond angles (presented in Table SI 3, ESI‡) are comparable to the DFT-calculated values of the angles N1–Pd–N5 (169.677°) and N3–Pd–Cl1 (164.264°) shown in Table 2. The **Pd2** cations pack as inversion dimers, with no metal–metal interactions as evidenced by a longer Pd–Pd distance (6.3601(6) Å) compared to the minimum separations distance (4 Å) required for effective intermetallic interactions.[35] However, there exist non-conventional intermolecular linkages through C20–H⋯Cl1 and C17–H⋯C9 as presented in Figure SI 22, ESI‡. These are mainly the weak van der Waals type. In addition, as illustrated in Figure SI 23, ESI‡, **Pd2** cations pack in columnar stacks, and the packing compares well with that reported in the literature for a related Pd(II) complex [5e].
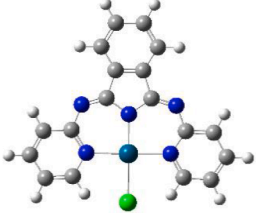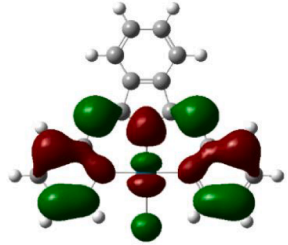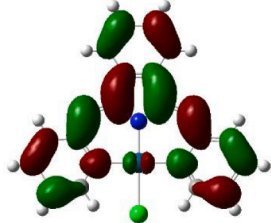
3.2. DFT analysis
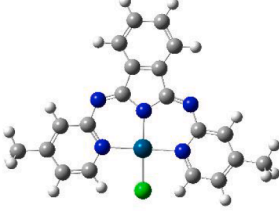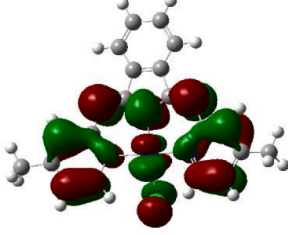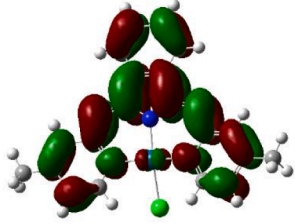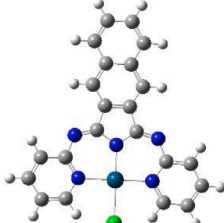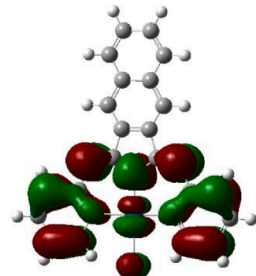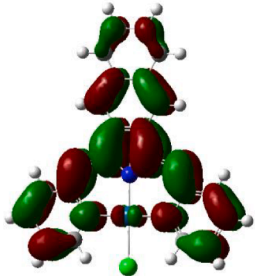
The geometry-optimized structures of the Pd(II) complexes, images of HOMOs, LUMOs, planarity and extracts of calculated data are shown in Tables 1 and 2, respectively.

The mappings of the frontier orbitals in Table 1 show that the LUMOs encompass the entire complex, while the electron isodensities of the HOMOs are projected predominantly 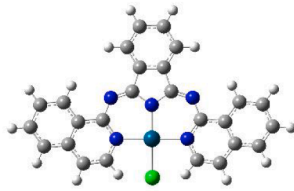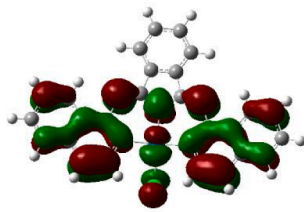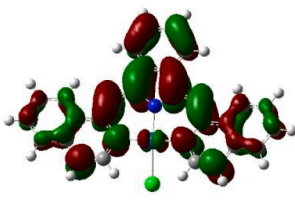over the bis(pyridyl)imino-2,5-pyrrolate moieties of the BPIs as well as Pd–Cl bond. These MOs are derived from the π-system of the bis(pyridyl)imino-2,5-pyrrolate of the BPIs, the 3p-orbitals of Cl atom as well as from 4d-orbitals of the Pd atom and seem to be dictating the magnitude of the HOMO energies.

The methylation in the 4/4′-positions at the lateral pyridyl rings of the BPIs raises the HOMO energy from −6.209 eV (for **Pd1**)) to −6.133 eV (for **Pd2**). Similarly, benzannulation of the lateral rings raises the HOMO energy from −6.209 eV (for **Pd1**) to −6.197 eV (for **Pd3**) and −6.104 eV (for **Pd4**). Thus, methylation of the lateral pyridines and benzannulation increase the electron density of the BPI core, leading to the destabilization of their HOMO energies. This is attributed to increased electron repulsions in the occupied molecular orbitals. The HOMOs' mappings for these complexes are comparable to those

Table 1

DFT optimized structures, HOMO and LUMO frontier molecular orbitals, and respective planarity for the Pd(II) complexes calculated using the B3LYP/LANL2DZ method (Isovalue = 0.02).

Complex structure	HOMO maps	LUMO maps	Planarity
Pd1			
Pd2			
Pd3			
Pd4			

reported for Pt(II) complexes [5c,8].

The LUMOs encompass π* MOs admixtures, derived from the phenyl moieties (for **Pd1**, **Pd2** and **Pd4**) or naphthyl (for **Pd3**) and the bis(pyridyl)imino-2,5-pyrrolate moieties.[8] There are only small contributions from the 4d-orbitals of the Pd atom. The interactions from the atomic orbitals incrementally raise the LUMO energy from −2.982 eV (for **Pd1**) through −2.917 eV (for **Pd2**) to −2.891 eV (for **Pd3**) while significantly lowering that of **Pd4** to −3.180 eV. For the latter complex, a lower HOMO-LUMO energy gap is observed compared to the other complexes. Therefore, it is observed that methylation of the lateral rings of the BPI leads to the destabilization of the LUMOs of **Pd2** while benzannulation results in destabilizing of **Pd3** and a contrasting stabilization of the LUMOs of **Pd1** and **Pd4**.

The angles around the Pd(II) centres show near-perfect square-planar coordination for **Pd1** and **Pd3**, while those for **Pd4** and **Pd2** show some significant deviations from linearity, culminating in non-linearity in the bite angles. The deviations are possible manifestations of steric conflicts

between the *ortho*-hydrogen atoms from the pyridyl rings of the respective BPIs and the chloride atoms of the latter complexes.[5c, 7] The HOMO-LUMO energy increases following the order: **Pd4** < **Pd2** < **Pd1** < **Pd3** (see Table 2). However, it does not correlate well with the observed reactivity trends and thus is of minimal effect on the rate of substitution.

3.3. Kinetics and mechanistic analysis

In the *pseudo* first-order situation, the substitution reaction of the labile chloride ligand from the Pd(II) complexes by the thiourea nucleophiles proceeded *via* two consecutive steps, denoted by observed rate constants, $k_{obs(1/2)}$ for all the complexes except for **Pd4** where only a single step was observed. The $k_{obs(1/2)}$ values were acquired by fitting absorbance-time data to standard single-exponential decay functions. Representative kinetic traces (absorbance-time data evolution) for the two substitution steps for the reaction between **Pd1** and **Tu** are

Table 2
Summary of calculated parameters for the Pd(II) complexes studied.

Property	Pd1	Pd2	Pd3	Pd4
NBO Charges				
Pd^{2+}	0.573	0.557	0.573	0.566
Cl^-	−0.545	−0.560	−0.544	−0.562
Electrophilicity index (ω)	6.544	6.366	6.245	7.400
Bond lengths (Å)				
Trans- N3–Pd	2.009	2.004	2.011	1.997
Cis- N–Pd	2.137	2.090	2.138	2.090
Pd–Cl	2.479	2.479	2.478	2.484
H⋯Cl	2.24	2.41	2.24	2.43
Energy gap (eV)				
LUMO (eV)	−2.982	−2.917	−2. 891	−3.180
HOMO (eV)	−6.209	−6.133	−6.197	−6.104
$\Delta E_{LUMO\text{-}HOMO}$	3.227	3.216	3.306	2.912
Bond angles (°)				
Trans N3 – Pd – Cl	179.998	164.264	179.989	162.572
Cis N1 – Pd – N5	178.764	169.677	178.999	169.027
Deviation of Pd – Cl from the main axis	0	13.13	0	34.56
Dipole moment (Debye)	3.445	4.765	4.677	6.687

presented in Fig. 3.

Average $k_{obs(1/2)}$ values of 6–8 runs (for reactions that were monitored using the stopped-flow analyzer) and 3 runs (for reactions monitored by the UV–visible spectrophotometer) were used for the linear regression of the data to obtain the second-order rate constants, presented as $k_{(1/2)}$. When the average values of $k_{obs(1/2)}$ were plotted against [Nu], with the aid of OriginPro 9.1® software,[36] straight-line plots having zero y-intercepts were obtained. The $k_{(1/2)}$ constant values were deduced from the regression slopes of the plots. The zero y-intercepts meant that the solvolysis or reverse pathway was insignificant or absent. Therefore, the substitution reaction proceeds by the rate law shown in equation (1).

$$k_{obs(1/2)} = k_{(1/2)}[Nu] \quad Nu = \mathbf{Tu}, \mathbf{Dmtu}, \mathbf{Tmtu} \qquad 1$$

Characteristic plots of $k_{obs(1/2)}$ against the concentration of the nucleophiles of **Pd3** are shown in Fig. 4a and b (see also similar plots in Figures SI 24–26 and SI 30–31, whereas the k_{obs} values for specific nucleophile concentration are shown in Tables SI 4–7 and Tables SI 12–14, ESI‡). The values of $k_{(1/2)}$ are listed in Table 3.

To get the thermal activation (enthalpy, $\Delta H^{\neq}$, and entropy, $\Delta S^{\neq}$) parameters for the substitution reactions, the rate constants which had been measured at different temperatures were linearly fitted according to the Eyring[37] equation (2),

$$\ln\left(\frac{k_{1/2}}{T}\right) = -\frac{\Delta H^{\neq}_{(1/2)}}{RT} + \left(23.8 + \frac{\Delta H^{\neq}_{(1/2)}}{R}\right) \qquad 2$$

where, T and R are the temperature of the reaction medium and gas constant, respectively. When the $ln\left(\frac{k_{(1/2)}}{T}\right)$ values were plotted against values of $\left(\frac{1}{T}\right)$ the values of activation parameters, $\Delta H^{\neq}$ and $\Delta S^{\neq}$ were obtained from the slopes and the y-intercepts of the plots, respectively. Typical Eyring plots for the reactions of **Pd4** with the nucleophiles are shown in Fig. 5.

In addition, similar plots are presented in Figures SI 27–29 and SI 32-SI 34, while the values of $ln\left(\frac{k_{(1/2)}}{T}\right)$ and $\left(\frac{1}{T}\right)$ are given in Tables SI 8–11 and Tables SI 15–17, ESI‡. The calculated values of $\Delta S^{\neq}$ and $\Delta H^{\neq}$ are summarized in Table 4.

A comparison of the respective values of k_1 and k_2 indicates that the values of the former rate constants are 3–4 orders of magnitude higher than those of the latter for the reactions of **Pd1-3**. The first substitution step is attributed to the nucleophilic substitution of the chloride coordinated to the Pd(II) complexes by the nucleophiles, whereas the slower one (which is the second reaction step) represents complete dechelation of the BPIs in rapid succession steps. These are induced by a labilizing effect of the coordinated thiourea upon substituting the chloride co-ligand and the isoindolate head at the *trans*-position. The ultimate products of the substitution reactions are the respective free BPI ligands and $Pd(Nu)_4^{2+}$ species. The dechelation of the BPIs was confirmed by monitoring the reaction of **Pd2** and **Tu** over time in tetrahydrofuran-d_8 solvent using ^{1}H NMR spectroscopy as shall be discussed ahead. Dechelation of tridentate ligands has also been observed for the reactions of some dinuclear Pt(II) complexes having a related tridentate N^N^N ligands coordination [38] and reactions of bidentately-coordinated dinuclear Pt(II) complexes.[39] The consecutive reaction pathway followed by all except **Pd4** is as depicted in Scheme 1, *vide infra*.

To verify the above-proposed reaction mechanism, **Pd2** was reacted with 6 equivalents of **Tu** and the changes experienced in the chemical shifts (δ) and intensity of the protons belonging to the coordinated 6-pyridyl of **L2** were monitored as a function of time. The ^{1}H NMR spectrum of **L2** and subsequent spectral arrays of the reaction mixture of the **Pd2** with 6 equivalents of **Tu** are presented in Fig. 6. The Hª' (H$^{6/6'}$) protons' resonance peak occurs as a doublet (d) at δ of 8.4 ppm and is upfield of the resonance peak of the same protons (Hª) for the **Pd2**, which occurs as a singlet at δ = 9.95 ppm (spectral data at t = 0 in the array). In the same spectrum, the absence of the N—H resonance of the isoindolate which occurs at δ = 14.1 ppm in the free ligand's spectrum
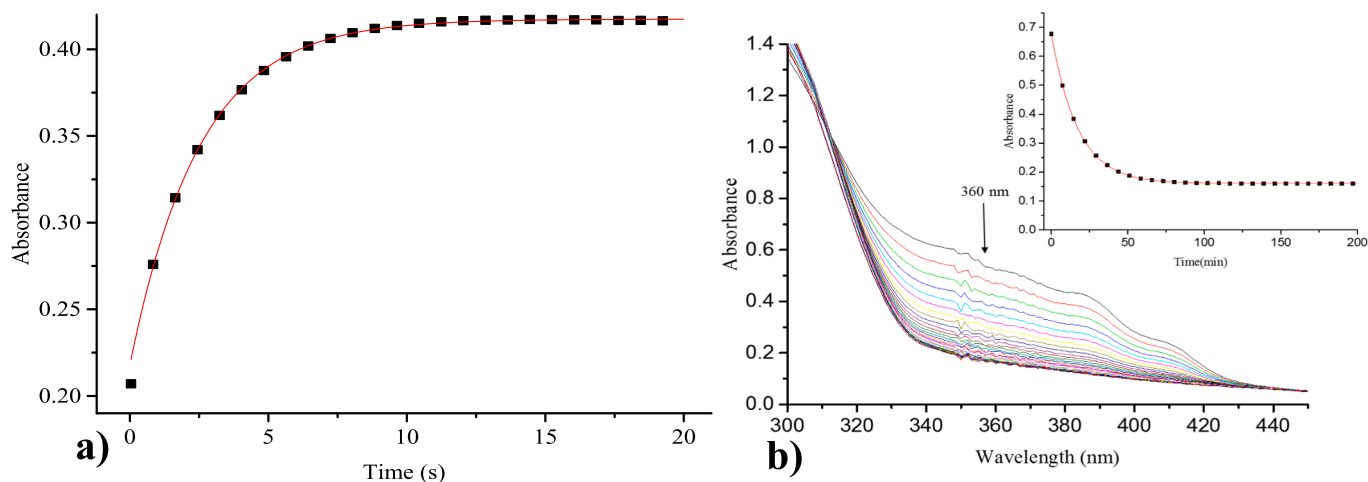
Fig. 3. a) Stopped-flow kinetic trace for the first step reaction of pd1 (1.0 × 10^{-4} M) with Tu (3.0 × 10^{-3} M) at 308 K and wavelength of 360 nm. **b)** UV–visible spectra for the second step reaction of Pd1 (1.0 × 10^{-4} M) with Tu (3.0 × 10^{-3} M) at 298 K. Inset: single exponential fitting of kinetic data at 360 nm.
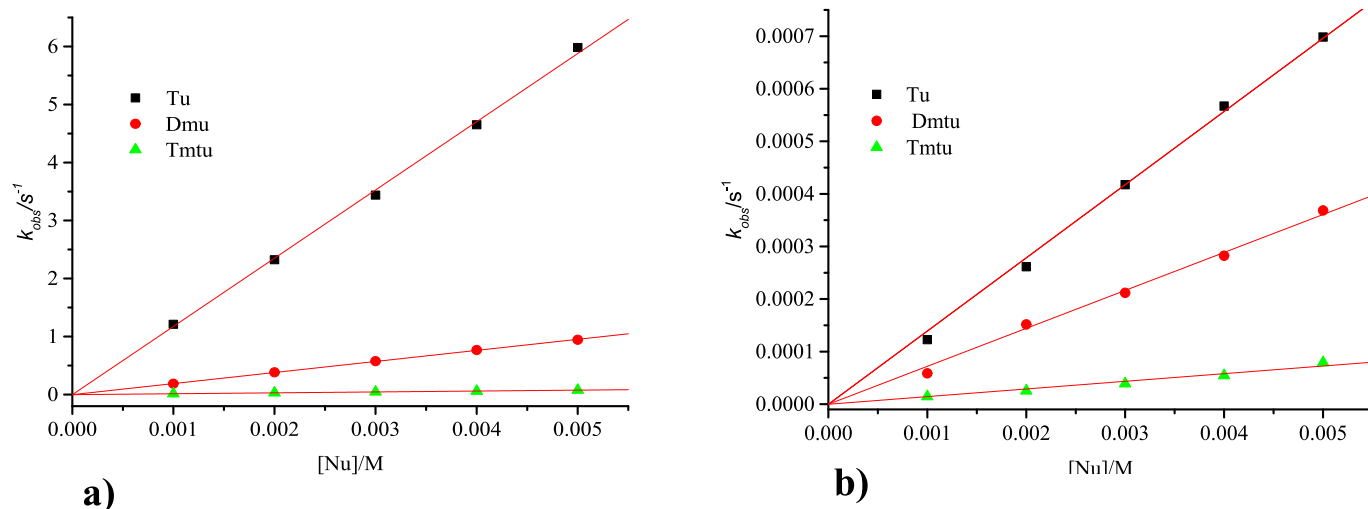
Fig. 4. Plots of $k_{obs(1)}$ (a) and $k_{obs(2)}$ (b) versus [Nu] for the substitution of chloride and the dechelation of **Pd3**, respectively, I = 0.01 M CF$_3$SO$_3$H, T = 298 K.

Table 3
The rate constants, k_1 and k_2 for the reactions between the Pd(II) complexes and thiourea ligands at T = 298 K.

Complexes	Nucleophiles	k_1 (M^{-1} s^{-1})	$k_2 \times (10^{-2}$ M^{-1} s^{-1})
Pd1	Tu	2046 ± 20	53.1 ± 0.6
	Dmtu	848 ± 7	39.5 ± 0.4
	Tmtu	319 ± 2	26.2 ± 0.3
Pd2	Tu	1322 ± 4	15.7 ± 0.3
	Dmtu	288 ± 2	12.1 ± 0.2
	Tmtu	69 ± 1	5.3 ± 0.2
Pd3	Tu	1176 ± 10	13.9 ± 0.2
	Dmtu	191 ± 1	7.2 ± 0.1
	Tmtu	15.6 ± 0.1	1.5 ± 0.1
Pd4	Tu	4.22 ± 0.03	–
	Dmtu	1.01 ± 0.01	–
	Tmtu	0.35 ± 0.004	–

No second step observed.

Table 4
Values of $\Delta H^{\neq}_{(1/2)}$ and $\Delta S^{\neq}_{(1/2)}$ for the chloride substitution from the Pd complexes.

Complexes	Nucleophiles	Enthalpy (kJ mol^{-1})		Entropy (J K^{-1} mol^{-1})	
		$\Delta H^{\neq}_1$	$\Delta H^{\neq}_2$	$\Delta S^{\neq}_1$	$\Delta S^{\neq}_2$
Pd1	Tu	33 ± 2	70 ± 1	−72 ± 7	− 49 ± 3
	Dmtu	50 ± 2	41 ± 1	−21 ± 8	− 132 ± 3
	Tmtu	41 ± 1	54 ± 1	−104 ± 5	− 71 ± 4
Pd2	Tu	56 ± 3	65 ± 3	− 25 ± 10	− 59 ± 9
	Dmtu	49 ± 1	60 ± 1	− 41 ± 3	− 80 ± 4
	Tmtu	51 ± 2	65 ± 1	− 50 ± 5	− 52 ± 3
Pd3	Tu	53 ± 2	59 ± 1	−20 ± 7	− 76 ± 2
	Dmtu	53 ± 1	57 ± 3	−19 ± 5	− 79 ± 8
	Tmtu	47 ± 1	61 ± 2	−65 ± 3	− 57 ± 6
Pd4	Tu	64 ± 2		−24 ± 7	
	Dmtu	66 ± 2		−27 ± 6	
	Tmtu	56 ± 1		−77 ± 3	

to the free **L2** ligand after its de-coordination from the complex by the three incoming **Tu** ligands in quick and successive steps. The intensity of the H^a protons of the complex decreases to almost zero in 22 h, whilst that (H$^{a'}$) of the corresponding free ligand (**L2**) increases in an inverse proportion. Thus, the observed time (22 h) frame for this exemplary reaction corroborates that the second and slower step observed for the reactions monitored on the UV–visible absorption spectrophotometer (denoted by the rate constant k_2) is a dechelation of the respective co-ordinated BPI ligand, leading to the ultimate formation of the Pd(Nu)$_4^{2+}$ and the respective free ligand as proposed in Scheme 1.

3.3.1. Insights into substitution reactions

The structures of the BPI ligands were altered via methylation and extending the π-conjugation, through benzannulation at different sites to the coordinated rings of the core BPI and the effect this caused on the reactivity of the complexes was measured. This was done to determine if the structural variations on the core BPI ligand could further slow the substitutional reactivity of the complexes as a design strategy to limit their susceptibility towards deactivation by biological nucleophiles.

Starting from the structure of the **Pd1**, a change was introduced onto the core BPI ligand by methylation of its lateral pyridyl rings to obtain **Pd2**. Benzannulation of the centrally coordinated isoindolate (*trans* to the Cl) gave **Pd3** while at the lateral pyridyl rings (*cis* to the Cl) formed **Pd4**. The k_1 data showed that the reactivity of **Pd2-4** towards chloride substitution by thiourea nucleophiles is lower than that of **Pd1**, giving further credence to the BPIs being a potential class of ligands for lowering the lability of their Pd(II) complexes. This is a requirement for
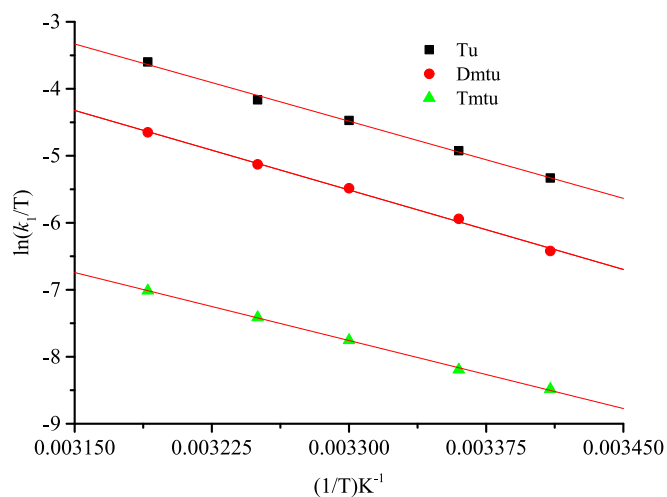

Fig. 5. Eyring plots for the reactions of Pd4 with thiourea nucleophiles at different temperatures.
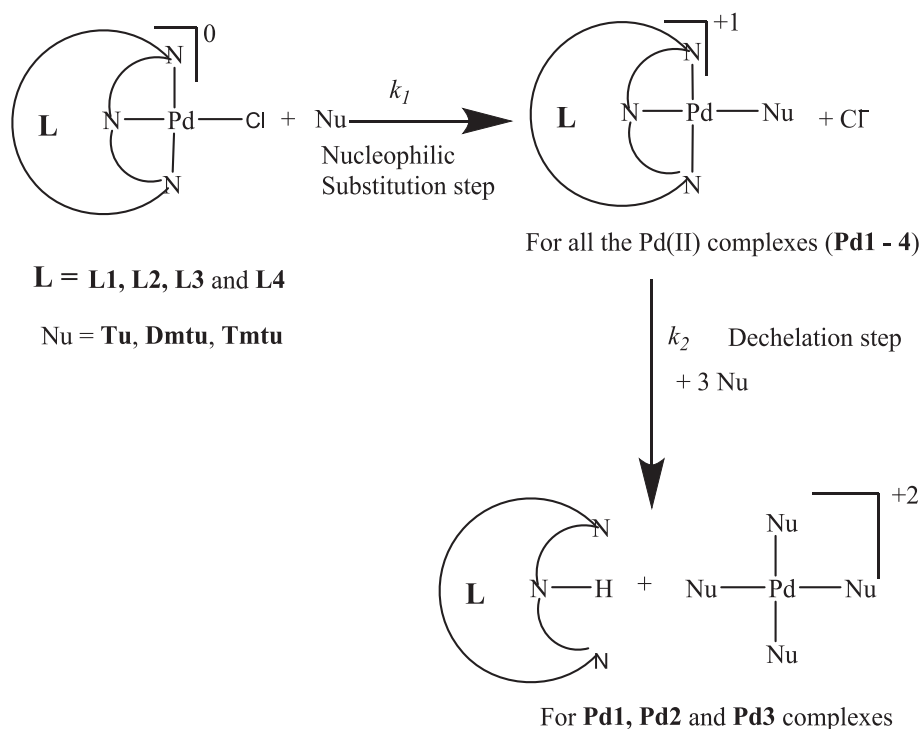
[7] is also noted.

In less than 4.5 min after the onset of the reaction, the evolved spectrum shows that the H^a protons at 9.95 ppm decrease in intensity and there is an emergence of two additional peaks at $\delta = 8.49$, (H$^{a'}$) and a broad-singlet at $\delta = 14.02$ ppm. The latter two resonance peaks are due

Scheme 1. Proposed reaction mechanism for the chloride substitution from the Pd(II) complexes.
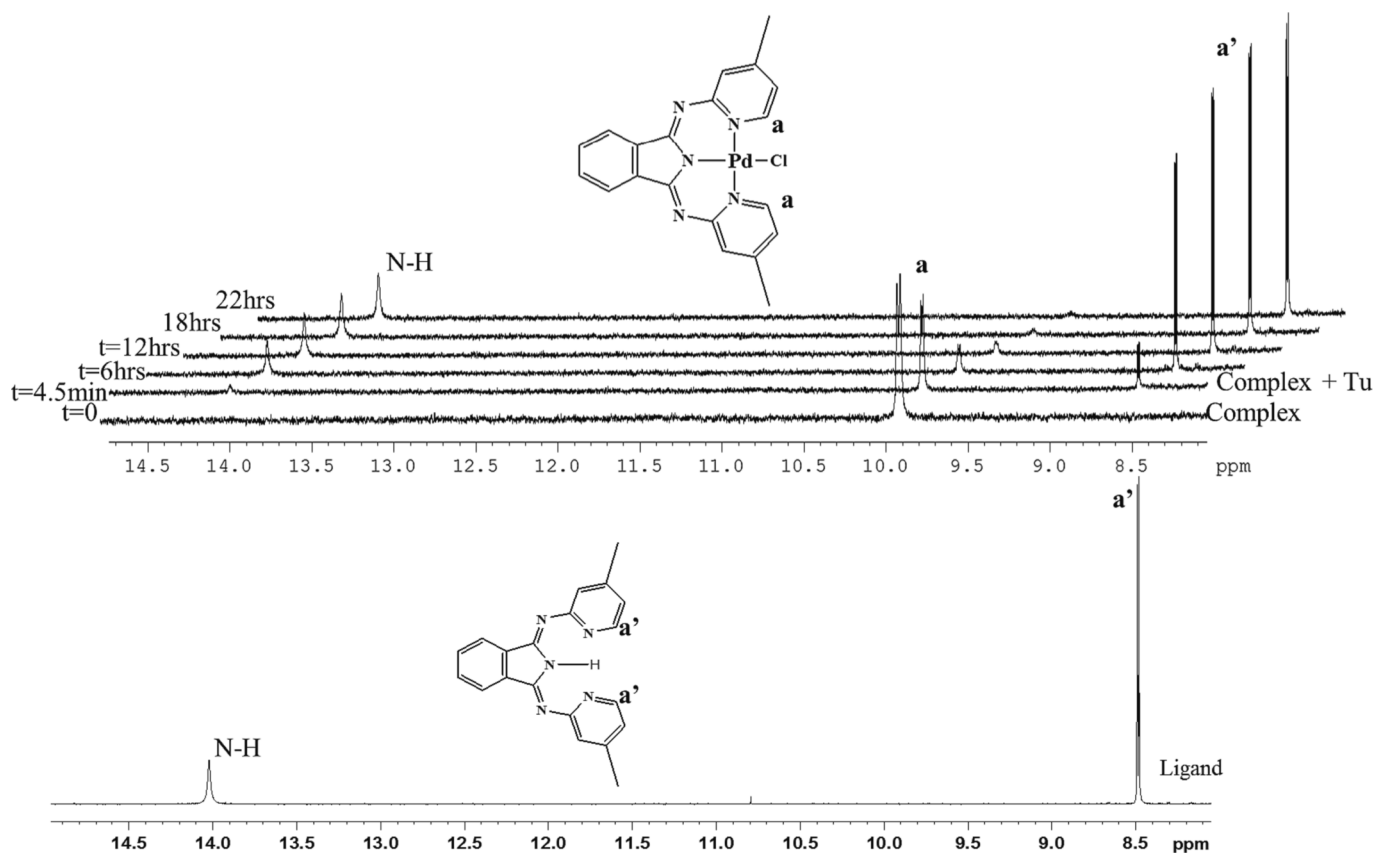
Fig. 6. The changes in the ^{1}H NMR spectrum for the reaction of Pd2 with Tu (6 equivalents) in tetrahydrofuran-d_8 with time. The complex undergoes complete dechelation within 24 hrs.

designing active Pd(II) complexes with reduced toxicity. How these structural variabilities affected the substitution rate of the leaving ligand is further discussed after this point.

The data from Table 3 show that the overall rate of direct chloride substitution from the Pd(II) complexes decreases following the order **Pd1 > Pd2 > Pd3 > Pd4** in the first step. A similar trend is also noted in the dechelation step for the complexes with an exception of **Pd4**.

A comparison of the k_1 values of **Pd1** and those of **Pd2** for all the nucleophiles used reveals that the latter's rate constants are decreased by factors in the range 2–5. The methyl substituents at the 4,4′-positions of the lateral pyridyl rings, being electron-donating groups,[13a] increase the electron density into the lateral (*cis*) pyridyl rings of BPI through inductive σ-donation. Increased density of electrons onto the *cis* Pd-N bonds reduces the positive charge density of the Pd metal which also reduces the rate of Cl substitution.[13b,30b], Methylation also weakens the π-acceptor ability property from the lateral pyridyl rings. This effectively isolates the pyridyl rings from the central isoindolate head, *vide supra*. Consequently, this lowers the π-back bonding of electrons from the metal's filled d-orbitals into the empty antibonding (π*) or nonbonding orbitals of the in-plane BPIs. The electrophilicity of the Pd(II) metal centre of **Pd2** is decreased. The trend in the electophilicity indices supports this fact because the value for **Pd1** is higher than for **Pd2** (Table 2). It is also evidenced that methylation at the 4,4′-positions of the *cis*-pyridyl rings for **Pd2** induces some steric in-plane repulsions at the Cl co-ligand. Compared to that of **Pd1**, the Pd–Cl bond is titled out of the plane by 13.13° (Table 2). This is caused by the repulsive interactions ($H^{6,6'}_{(py)}$···(Cl)PdN$_3$, d_{min} = 2.41 Å) between the Cl co-ligand and the $H^{6,6'}$ (*ortho*-hydrogens) of the lateral pyridines of **Pd2**, which is more than that of **Pd1** ($H^{6,6'}_{(py)}$···(Cl)PdN$_3$, d_{min} = 2.24 Å).

Similar comparisons with **Pd1** showed that the k_1 values for reactions of **Pd3** and **Pd4** with **Tu** are lower by factors of about 2 and 500, respectively. This is contrary to what would be expected of most square-planar Pt/Pd(II) complexes which are coordinated with tridentate ligands that have extended π-conjugation, especially the pyridyl-type. Such an unexpected trend was also reported in the study by Wekesa and Jaganyi.[10] Moreover, literature data for square-planar Pt(II) complexes[5c, 8] indicated that the energy bandgap and hence the absorption frequency corresponding to the metal-to-ligand (intra-ligand) charge transfer (ML/ILCT) increased in the order **L4** < **L1** < **L3**. This also agreed with the trend in the reduction potentials of the free ligands. The trends in the literature data meant that **L4** ligand was a stronger π-acceptor than the other three. In this case, one would expect **Pd4** to be more reactive than the rest, yet the trend in the k_1 values shows the opposite.

The 500-fold reduction in the reactivity of **Pd4** relative to that of **Pd1** suggests that both the electronic and a possible overbearing steric effect are at play. Benzannulation at the lateral pyridines of BPIs (to form isoquinolines / benzopyridines) as donor rings strengthens the π-donation of these moieties towards the Pd metal centre contrary to expectation based on increased π-surface areas of the ligand at the *cis* positions. Thus, the extension of the semi-isolated pyridyl rings by co-joining them to a strong phenyl ring (benzannulation) effectively weakens their π-acceptor properties. As a result of a stronger electron π-donation of **L4** towards the central Pd metal via the Pd-Cl *cis* bonds, the metal's electrophilicity index is lowered, leading to unusually lower substitution rates. This anomaly in the rate of substitution has been reported by our group.[14a,14b,40] Because the extent of retardation on the rate is so large, it is conceivable that steric shielding of the leaving group by proximal coordinated rings may also be an important retardation factor. As explained for the effects of structural changes enacted via 4,4′-methylation of the lateral pyridyl rings, benzannulation at the *cis*-pyridyl rings for **Pd1**, respectively introduces in-plane steric effects on the Pd-Cl bond. The *cis*-positioned isoquinolines being more steric demanding groups cause stronger mutual repulsions/conflicts between their proximal *ortho*-hydrogens and the Cl co-ligand (H···Cl, d_{min} = 2.43 Å, see Table 2). As a result, the Pd–Cl bond for **Pd4** tilts out of the ClPdN$_3$

plane by as much as 34.56°. A look at the planarity of **Pd4** (Table 2) depicts that the Pd–Cl fragment experiences the strongest out-of-plane distortions. This causes steric hindrance to the entering nucleophile on one side of the plane, which significantly lowers the substitution rate for **Pd4**.

Benzannulation at the centrally coordinated isoindolate also yields an unexpected effect on the reaction rate. One would expect that adding a phenyl ring to the isoindolate head of **Pd3** would make it more reactive compared to **Pd1** if increased π-surface or the associated *trans*-labilization effect is the crucial determining factor. However, this structural change in the ligand framework lowers reactivity by about half compared to **Pd1**'s data. It is unclear why this opposite trend is observed. However, what seems probable is that the effect on the rate due to changes in the ligand structure is derived from the anomalous structure of **L3**, either in the ground or the transition state of its complex upon being thermally activated. Comparison of the DFT calculated Pd-Cl bond lengths for the two complexes rules out a ground state *trans* effect as the controlling factor. A proposition is that the anomalous effect on the rate is stemmed from the significant mismatch in the energies of the orbitals parentage of the deprotonated bis(pyridyl)imino-2,5-pyrrolate and the naphthalinyl moieties of the **L3** ligand. This is also evidenced by the high energy bandgap in the ground states of the **Pd3**. As already alluded to, **L3** has *pseudo*-π-conjugated and extended MOs delineated by the nodal points located on the 2,5-imino bridges of the pyrrolate head. Therefore, an extension of the π-surface of the 1,3-bis(pyridyl)iminoisoindolate by phenyl attachment does not enhance the π back-donating ability of the entire ligand. This makes it an unusually weaker π-acceptor ligand. Thus, when this ligand is coordinated to the central Pd atom, the expected synergism between its π-acceptor capacity and its anionic isoindoline (a strong σ-donor) is not effectively realized. Theoretically, the synergism would increase the Pd(II)'s positive charge as the ligand's conjugated π-surface was increased. This would make **L3** a stronger *trans* σ-activator, leading to increased rates in the ground state. Contrary to expectations, lower rates were measured for **Pd3** with all nucleophiles. In other words, in the transition state, **Pd1** is more electrophilic than **Pd3**, hence the higher observed reactivity for the former.

The BPI ligands of the Pd complexes, except that from **Pd4** were dechelated from the metal centre in a subsequent step that was 2-/3-folds lower than the first. The dechelation step presents two possibilities. Either the nucleophile which substituted the Cl co-ligand eventually labilized the deprotonated isoindolate unit first, followed by the slow substitution of the pyridyl units by two more nucleophiles. Such a *trans*-effect by thioureas has been reported in the dechelation of some dinuclear Pt(II) complexes.[39a,41] The intermediate Pd(II) metallocycle that results has two *trans*-configured and hemi-labile N$_{py}$–Pd bonds which can be substituted rapidly by two more **Tu** nucleophiles. The final products would be a free BPIs ligand and a [Pd(Nu)$_4$]$^+$ species.

The second possibility is linked to the steric hindrance of the already coordinated **Tu** (compared to the displaced Cl) from the first step, which would lead to the substitution occurring first at one of the lateral pyridyl units of the BPIs instead of the isoindolate head. A similar mechanism was observed for the reactions of some terdentate dinuclear Pt(II) complexes having relatively flexible N^N^N ligands [38a,42]. The last two incoming thioureas would then rapidly substitute the N atoms of the pyridyl and the isoindolate head either simultaneously or in rapid succession to form the same products as aforementioned.

On the other hand, the absence of dechelation in **Pd4** may be due to its ligand (**L4**) being the strongest π-acceptor of the four.[5c, 8] This makes it a good candidate for withdrawing electron density from the metal orbitals. The interactions between the metal's d-orbitals with the ligand's p-orbitals are thus enhanced, resulting in the shortening of the Pd–N3 bond compared to other complexes, making it harder for the ligand to detach from the Pd metal.

The rate of chloride substitution from the Pd(II) complexes showed a dependence on the bulkiness and thus steric hindrance of the S-donor atoms of the incoming nucleophiles as evident from the trend in the rate

constants shown in Table 3. The thiourea nucleophile substituted the chloride co-ligand in the order: **Tu > Dmtu > Tmtu**. This trend reflects the steric bulk of the nucleophile, with the bulkiest nucleophile, **Tmtu** (which has four methyl groups around the S-donor atom) being the slowest in attacking the Pd(II) metal ion while the unsubstituted **Tu** is the fastest. The trend is also reported in the literature for other associatively-activated ligand substitution reactions. [13b,43] For all nucleophiles, the reactions proceeded *via* a bond-forming activated pathway as evidenced by the negative values of the activation entropies ($\Delta S^{\neq}_{1/2}$) and the relatively low enthalpies ($\Delta H^{\neq}_{1/2}$). This is archetypical of an associative substitution mechanism, known for substitution from square-planar d^8 complexes. [44].

3.4. CT-DNA binding

3.4.1. Electronic absorption titrations

The electronic absorption spectra of the complexes (**Pd1-Pd4**) showed well-resolved bands in the range of 290–500 nm. A typical change in absorbance accompanying titrating the complexes with CT-DNA is shown in Fig. 7 for **Pd1** (similar spectra for **Pd2-Pd4** are presented in Figures SI 35 – 37, respectively). The interactions of the complexes with the increasing amounts of CT-DNA are measurable at 350 nm since these intra-ligand charge transfer transitions of the type π → π* and n → π* for the coordinated ligands are sensitive to all ant form of non-covalent interactions between the complexes and the host, DNA. [45] Resultantly when the concentration of DNA is increased, there is a concomitant decrease in molar absorbance (hypochromism, 30–40 %) for the Pd complexes. This suggests associative interaction that can be adsorptively, intra-base intercalation, or grove binding. The values of intrinsic binding constants, K_b are moderately large and follow the order: **Pd1 > Pd2 > Pd3 > Pd4** (Table 5). The order is consistent with the trend for chloride substitution. The magnitude of K_b (10^5 M^{-1}) values compares reasonably well with similar Pd complexes reported in the literature.[31d,31e,46] The negative sign of the values of ΔG shows the spontaneity of the associative interactions of the complexes with DNA.[31e].

3.4.2. Fluorescence quenching

To further confirm the mode and extent of interactions of the complexes with DNA, the fluorescence emission of EB/CT-DNA in the absence and presence of an increasing concentration of the Pd
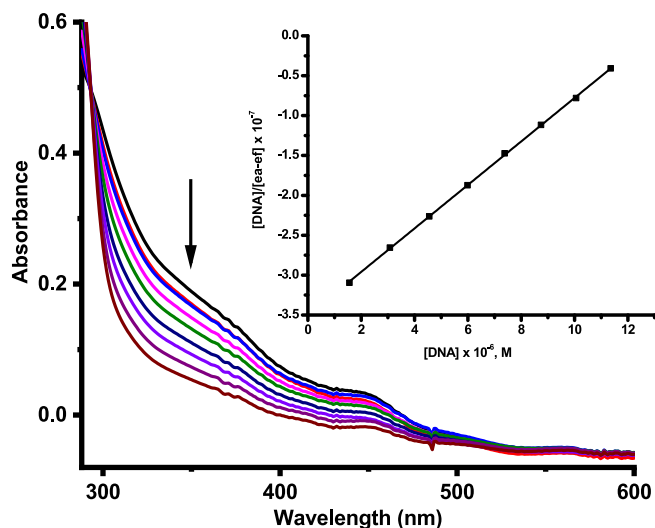

Fig. 7. Absorption spectral changes of Pd1 in the presence of increasing concentrations of DNA. The arrows show the decrease in the intensity of absorption with the increasing amounts of DNA concentration. The inset graph shows the plot of [DNA]/[$\varepsilon_a - \varepsilon_f$] *vs* [DNA].

Table 5

DNA-binding constants derived from UV–Visible absorption and EB-DNA fluorescence titrations of the Pd(II) complexes.

| Complex	UV–Vis titration		Fluorescence emission titration				
	K_b (10^4 M^{-1})	$\Delta G^{\neq}_{25°C}$/ k Jmol^{-1}	K_{SV} (10^4 M^{-1})	K_{app} (10^6 M^{-1})	k_q (10^{12} M^{-1} s^{-1})	K_F (10^2 M^{-1})	n
Pd1	8.21 ± 0.4	−28.04	4.92 ± 0.2	2.31 ± 0.1	4.92 ± 0.2	11.02 ± 0.7	1.14
Pd2	7.58 ± 0.4	−27.83	4.77 ± 0.2	1.89 ± 0.1	4.77 ± 0.2	7.23 ± 0.6	0.99
Pd3	6.35 ± 0.3	−27.40	3.96 ± 0.2	1.67 ± 0.2	3.96 ± 0.2	1.94 ± 0.1	0.93
Pd4	4.98 ± 0.3	−26.80	3.02 ± 0.1	1.01 ± 0.2	3.02 ± 0.1	1.22 ± 0.1	0.92

complexes were monitored in the range 530–700 nm. These are shown in Fig. 8 (**Pd1**) and Figures SI 38- SI 40, for **Pd2-Pd4**, respectively. The emission intensity at 610 nm showed a considerable decrease (hypochromism) in intensity.[47] K_{SV} values of 4.92×10^4 M^{-1} for **Pd1**, 4.77×10^4 M^{-1} for **Pd2**, 3.96×10^4 M^{-1} for **Pd3** and 3.02×10^4 M^{-1} for **Pd4** are lower than that of EB (10^7 M^{-1}), illustrating that the complexes bind less strongly than EB (a classical DNA intercalator). The magnitude of the apparent association constants, K_{app} ($1.67–2.81 \times 10^6$ M^{-1}) are comparable to those of known comparative metallo-intercalators (10^7 M^{-1}), indicating that the complexes bind as intercalators of DNA than groove binders.[48] The bimolecular quenching rate constant k_q (magnitude 10^{12} M^{-1} s^{-1}) is higher than the maximum scatter-collision rate constant for known associative biopolymer (2×10^{10} M^{-1} s^{-1}), suggesting the existence of ultrafast associative interactions, dictated by a static quenching equilibrium.[49] However, the K_F values (magnitude 10^2 M^{-1}) portray moderately strong interactions of the complexes with DNA. The calculated n values are near unity, suggesting the existence of a single binding site per complex per base pair of DNA. The binding constants of the complexes on DNA follow the order **Pd1 > Pd2 > Pd3 > Pd4** and match the trend of their chloride substitution from the complexes (Table 3).

3.5. BSA-pd complex interactions

To understand the interaction of the Pd complexes with proteins, particularly serum proteins, BSA was chosen as the model due to its close structural resemblance to human serum albumin and good binding abilities.[50] The emission of BSA due to the tryptophan (Trp) amino acid residues (Trp-212 and Trp-134 in the subdomains IIA and 1B), respectively)[31c,51] was monitored at 320 nm by recording the spectra from 300 to 420 nm at increasing concentration of the Pd complexes. The spectra are shown in Fig. 9 for **Pd1**, and Figures SI 41-SI 43 for **Pd2-Pd4**, respectively. The emission intensities of Trp (of the BSA) show a notable decrease with increasing concentration of the complexes (ca. 30%). The observed hypochromicity is ascribed to non-covalent interactions that significantly change the tertiary structure of BSA as a result of the intricate changes in the immediate environment of the Trp residues. The $K_{SV(BSA)}$ values (Table 6 which are of the order 10^5 M^{-1}) are two orders of magnitude lower than those of classical intercalators (10^7 M^{-1}). [31d] The magnitude of the K_{SV} values depicts strong interactions of the complexes with BSA and this occurs mainly within the hydrophobic pockets of the host.[52] The k_q values of $0.76–3.67 \times 10^{12}$ M^{-1} s^{-1} are greater than those reported for known associative biopolymer (2.0×10^{10} M^{-1} s^{-1}), suggesting ultrafast kinetics for the associative interactions, governed by a static quenching mechanism. [53] The K_F values (magnitude 10^6 M^{-1}) are lower than the association constant (10^{15} M^{-1}) for irreversible interactions, revealing that complexes reversibly bind onto BSA.[54] Also, the K_F values show that the interactions are predominantly situated within the subdomain IIA of BSA (hydrophobic cavity *via* nonpolar residues).[55] The values of n
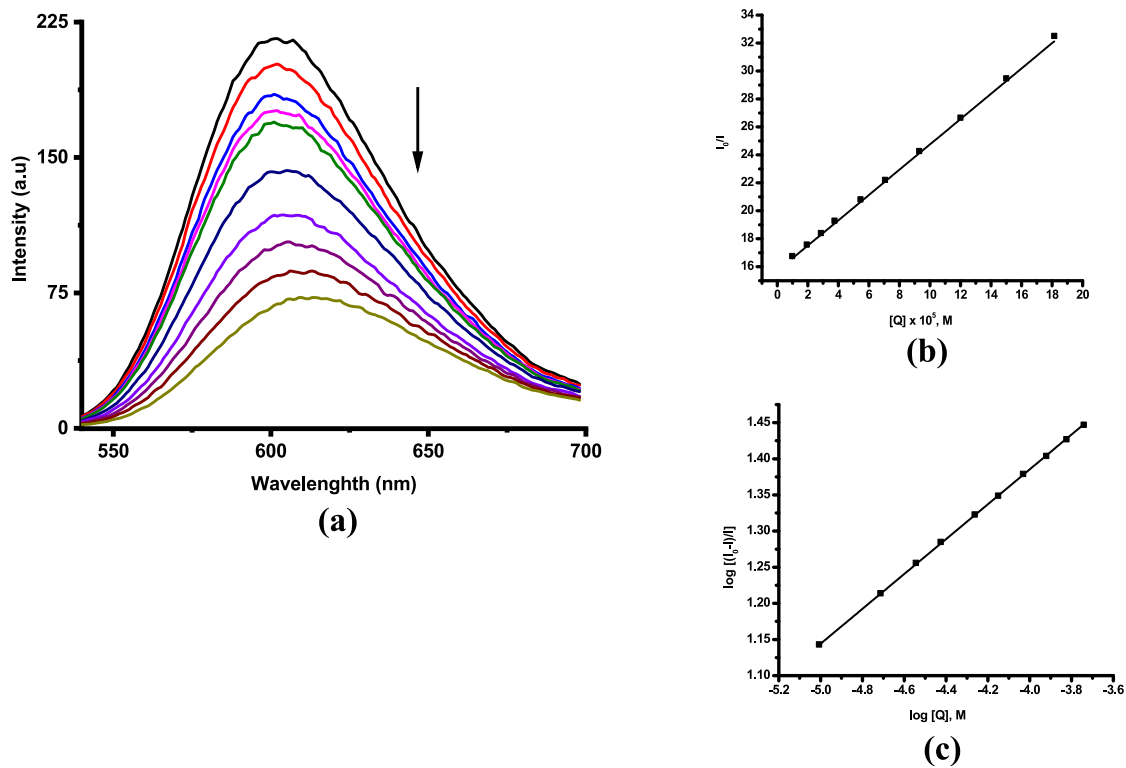
Fig. 8. (a) The steady-state fluorescence quenching spectra for EB-DNA in the presence of increasing amounts of **Pd1**. The arrow indicates the decrease in the emission intensity upon increasing the DNA concentration; **(b)** Stern – Volmer plot of I_0/I *vs* [Q]. **(c)** Scatchard plot of $\log[(I_0 - I)/I]$ *vs* $\log[Q]$.
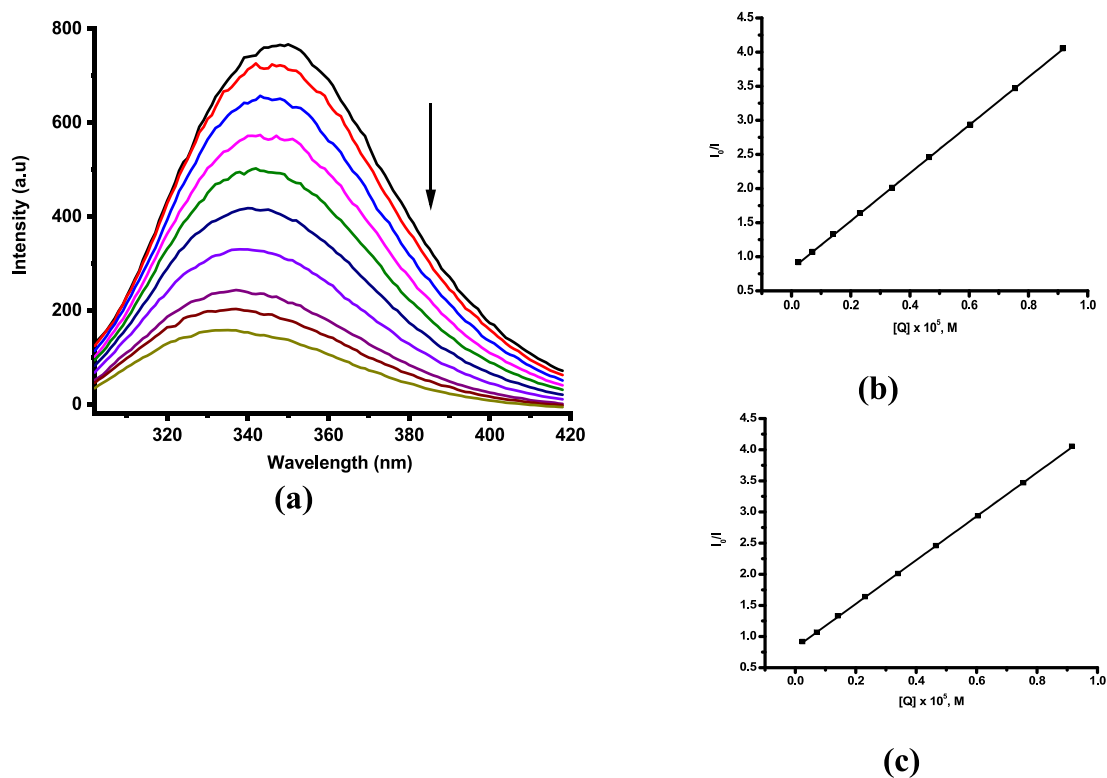
Fig. 9. (a) The emission profile of BSA in the presence of increasing amounts of **Pd1**. The arrow shows the decrease in the emission intensity with the increasing concentration of metal complexes; **(b)** Stern-Volmer plot of I_0/I *vs* [Q]; **(c)** Scatchard plot of $\log[(I_0 - I)/I]$ *vs* $\log[Q]$.

Table 6
BSA binding constants, and number of binding sites for the complexes.

Complex	$K_{SV} \times 10^5$, M^{-1}	$k_q \times 10^{12}$, M^{-1} s^{-1}	$K_F \times 10^6$, M^{-1}	n
Pd1	3.67 ± 0.2	3.67 ± 0.2	11.62 ± 0.4	1.33
Pd2	1.54 ± 0.1	1.54 ± 0.1	7.88 ± 0.4	1.11
Pd3	1.01 ± 0.1	1.01 ± 0.1	0.95 ± 0.1	1.20
Pd4	0.76 ± 0.1	0.76 ± 0.1	0.71 ± 0.1	1.01

which is close to 1, depict the presence of a single binding per molecule of BSA.

3.6. Molecular docking of the complexes

3.6.1. Modelling the DNA binding

Molecular docking simulations were conducted to better understand the interactions of the complexes with DNA as depicted in Table 7.

The results suggest that the compounds adsorptively bind to nucleotide residues in the minor groove of the DNA double helix. DA6, DA17 and DG16 nucleotide moieties participate in non-conventional hydrogen bond interactions with **Pd1**, **Pd2** and **Pd3**, respectively. Similarly, C—H bond interactions are observed with DT7 (for **Pd1**) and DG12 and DC11 (for **Pd2**). Also, a single triangular donor–donor interaction (DG16) stabilizes **Pd2** in the groove. **Pd4** exhibits one π-anionic interaction with
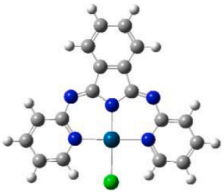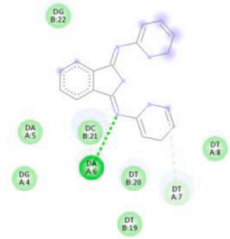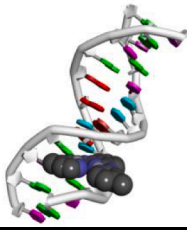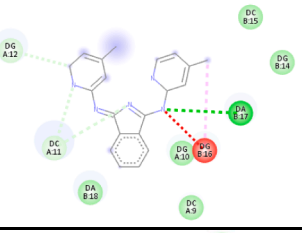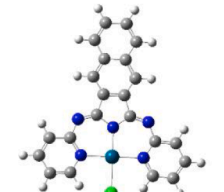
the DC23 nucleotide. The binding is further strengthened by the van der Waals forces formed between the complexes' ligand moieties and nucleotides such as DA5, DA6, DA17, DA18, DC9, DC11, DC15, DC21, DG4, 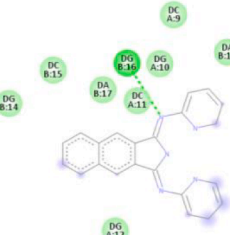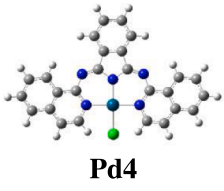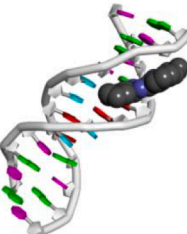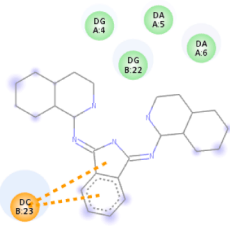DG10, DG14, DG22, DG24, DT7, DT8, DT19, and DT20. **Pd3** formed the most stable associative adduct with a binding energy (stability score) of −9.8 kcal/mol, while the DNA-**Pd1** adduct was the least stable with a binding energy (stability score) of −8.4 kcal/mol (Table 7). The trend contrastingly correlates with the experimental results (Table 5**)**.

The docked poses illustrate possible interactions of the Pd complexes with DNA. The minimum energy docked conformations show a preferred minor groove binding of the complexes onto DNA (with top-ranked poses). The interactions are distinguished by colored dotted lines. Molecular interactions include; pi-anion, conventional hydrogen bond, C—H bond, pi-alkyl, and triangular donor–donor. The more negative the binding score, the stronger the binding affinity between DNA and the complex (**Pd1-Pd4**).

3.6.2. Modelling the BSA interactions

To further gain insight into the interactions (putative active pocket, binding affinities, and mechanism) of the complexes with proteins biomolecular docking simulation onto BSA was carried out. Figure SI 44 illustrates the interactions which are dominated by hydrophobic

Table 7
DNA-Pd(II) complexes interactions showing the optimized poses and their energies. Docking data analyzed by discovery studio client visualizer.

Complex	Best docked poses diagram	2D Interaction diagram	Docking score (kcal/mol)
Pd1			-8.4
Pd2			-9.3
Pd3			-9.8
Pd4			-8.7

interactions (π-alkyl) as affirmed for the DNA and affirms the spectroscopic titration data. The binding sites for the insertion of the complexes onto BSA are dominated within the hydrophobic cavities for site 1 (subdomain IIA). The interactions of the BSA receptor with **Pd1**-**Pd4** are presented in Fig. 10. The pose of **Pd1** depicts it surrounded by hydrophobic amino acid residues such as ARG196, PRO110 (*via* pi-cation and anion interactions) and HIS145, ARG458 (*via* π-alky and alkyl interactions). The most stable pose of **Pd2** shows mutual interactions with amino acid residues: ILE455, ALA193, ARG196 and PRO 110 (alkyl and π-alkyl interactions); ASP108 and ARG144 (conventional hydrogen bond interactions); HIS145 and ARG458 (π-cation interactions), and GLU424 (pi-donor hydrogen bond). Similarly, **Pd3** has interacted associatively with ALA193, ARG196, LYS431, TYR451 and ILE455 (alkyl and π-alkyl); HIS145 (π-donor hydrogen bond); and SER (conventional hydrogen bond). Also, alkyl and π-alkyl (ILE455, ALA193, ARG196 and ARG144), π-cation and anion (GLU424 and ARG458), and carbon hydrogen bond (HIS145) interactions exist in **Pd4**. The obtained docking score of − 9.8, − 10.3, − 10.5, and −11.3 kcal/mol for **Pd1**, **Pd2**, **Pd3** and **Pd4** (respectively), and differed from the trends observed for the spectroscopic titrations.

4. Conclusions

The results from this study have demonstrated that it is possible to control the lability of Pd(II) complexes with a careful structural modification of a series of BPI ligands with varied electronic and steric qualities. Methylation of the lateral pyridyl units of the BPIs reduced the reactivity of their respective Pd(II) complexes but in a moderate manner. Benzannulation on the *cis*-pyridyl units was the most effective in reducing the substitution rate from the Pd(II) metal centre than placing a phenyl ring at the back of the *trans* isoindolate head. An increase in the *cis* π-donation, as well as steric shielding of the leaving group by the *cis*-coordinated and high surface-demanding isoquinolinyl groups, induce an in-plane H⋯Cl steric repulsions. This distorts the planarity of the complex, leading to significantly lower rates (2-/3-folds) than **Pd1** for the chloride substitution from **Pd4** by all nucleophiles. Benzannulation on the *trans*-position coordinated isoindolate did not induce distortions on the planarity of **Pd3**. However, a moderate fall in the rate was observed possibly due to the poor π-accepter property of its ligand as a result of an energy mismatch of the orbitals parentage forming the extended MOs of **L3**. The trend in the reactivity is opposite to that of the increasing π-surface which was a result of the destabilization of the HOMOs as demonstrated in trends of the DFT calculated data. All the complexes undergo dechelation except **Pd4**, a clear indication that these types of Pd(II) complexes might show instability in some biological fluid systems having a high temporal concentration of S-containing bionucleophiles. However, the stability of **Pd4** may make it a classic candidate for applications in such biological systems. The reaction mechanism is associative as confirmed by the decrease in the entropy from reactants to products. DNA titration data suggest moderately strong binding, with molecular docking showing minor groove binding. BSA spectroscopic titrations of the complexes, along with their docking simulations demonstrate that the complexes bind within the hydrophobic cavity of the protein. Complexes **Pd1**-**Pd4** illustrated a positive correlation between the rates of substitution kinetics, and DNA/BSA binding constants.

Funding

This work was funded by the University of KwaZulu-Natal, South Africa.

Declaration of Competing Interest

The authors declare that they have no known competing financial interests or personal relationships that could have appeared to influence
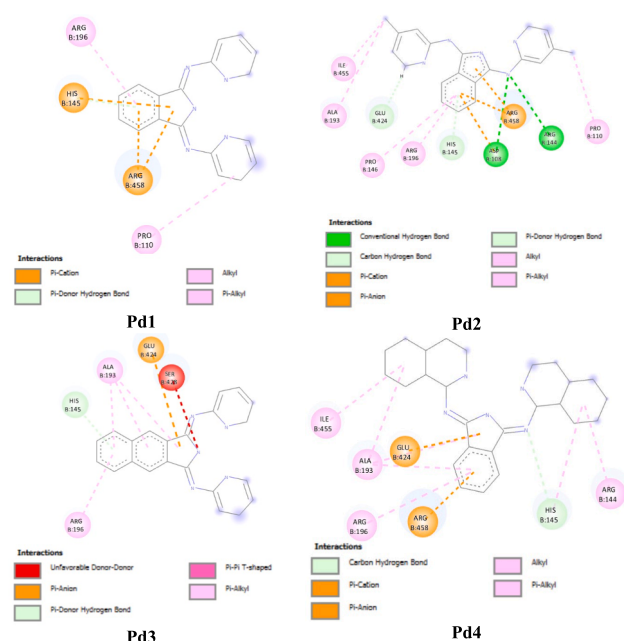

Fig. 10. 2D interaction diagram of **a** (**Pd1**), **b** (**Pd2**), **c** (**Pd3**) and **d** (**Pd4**) showing the observed interactions between amino acid residues and ligands' atom. Respective binding energy affinities are − 9.8, −10.3, −10.5, and −11.3 kcal/mol.

the work reported in this paper.

Data availability

Aditional data used is shared in the supplementary information attached files

Appendix A. Supplementary data

Supplementary data to this article can be found online at https://doi.org/10.1016/j.ica.2023.121730.

References

[1] a) Ž.D. Bugarčić, J. Bogojeski, R. van Eldik, Coord. Chem. Rev. 292 (2015) 91–106;
b) D.O. Onunga, R. Bellam, G.K. Mutua, M. Sitati, M.D. BalaKumaran, D. Jaganyi, A. Mambanda, J. Inorg. Biochem. 213 (2020) 111261.
[2] a) A.S. Abu-Surrah, M. Kettunen, Curr. Med. Chem. 13 (2006) 1337–1357;
b) M. Marques, ISRN Spectroscopy 2013 (2013) 1–29.
[3] a) D. Wang, S.J. Lippard, Nat. Rev. Drug Discov. 4 (2005) 307–320;
b) N.P. Barry, P.J. Sadler, Chem. Commun. 49 (2013) 5106–5131;
c) J. Bogojeski, J. Volbeda, M. Freytag, M. Tamm, Ž.D. Bugarčić, Dalton Trans. 44 (2015) 17346–17359;
d) S. van Zutphen, J. Reedijk, Coord. Chem. Rev. 249 (2005) 2845–2853;
e) H. Zorbas, B.K. Keppler, Chembiochem 6 (2005) 1157–1166.
[4] a) J. Elvidge, R. Linstead, Journal of the Chemical Society (Resumed) (1952) 5000–5007;
b) J. Elvidge, R. Linstead, Journal of the Chemical Society (Resumed) (1952) 5008–5012;
c) P. Clark, J. Elvidge, R. Linstead, Journal of the Chemical Society (Resumed) (1953) 3593–3601.
[5] a) K. Hanson, L. Roskop, N. Patel, L. Griffe, P. I. Djurovich, M. S. Gordon, M. E. Thompson, *Dalton Transactions* **2012**, *41*, 8648-8659; b) B. L. Dietrich, J. Egbert, A.

M. Morris, M. Wicholas, O. P. Anderson, S. M. Miller, *Inorganic Chemistry* **2005**, *44*, 6476-6481; c) K. Hanson, L. Roskop, P. I. Djurovich, F. Zahariev, M. S. Gordon, M. E. Thompson, *Journal of the American Chemical Society* **2010**, *132*, 16247-16255; d) M. B. Meder, L. H. Gade, *European Journal of Inorganic Chemistry* **2004**, *2004*, 2716-2722; e) M. Meder, C. H. Galka, L. H. Gade, *Monatshefte für Chemie/Chemical Monthly* **2005**, *136*, 1693-1706; fR. R. Gagne, D. N. Marks, *Inorganic Chemistry* **1984**, *23*, 65-74.

[6] a) D. M. Baird, W. Maehlmann, R. D. Bereman, P. Singh, *Journal of Coordination Chemistry* **1997**, *42*, 107-126; b) J. D. Dang, T. P. Bender, *Inorganic Chemistry Communications* **2013**, *30*, 147-151; c) B. K. Langlotz, J. Lloret Fillol, J. H. Gross, H. Wadepohl, L. H. Gade, *Chemistry-A European Journal* **2008**, *14*, 10267-10279; d) A. Scheja, D. Baabe, D. Menzel, C. Pietzonka, P. Schweyen, M. Bröring, *Chemistry-A European Journal* **2015**, *21*, 14196-14204.

[7] B. Siggelkow, M.B. Meder, C.H. Galka, L.H. Gade, Eur. J. Inorg. Chem. 2004 (2004) 3424–3435.

[8] H.-M. Wen, Y.-H. Wu, Y. Fan, L.-Y. Zhang, C.-N. Chen, Z.-N. Chen, Inorg. Chem. 49 (2010) 2210–2221.

[9] a) I. Sović, S.K. Pavelić, E. Markova-Car, N. Ilić, R. Nhili, S. Depauw, M.-H. David-Cordonnier, G. Karminski-Zamola, Eur. J. Med. Chem. 87 (2014) 372–385;
b) I. Sović, V. Stilinović, B. Kaitner, S. Kraljević-Pavelić, M. Bujak, K. Čuljak, P. Novak, G. Karminski-Zamola, J. Mol. Struct. 1006 (2011) 259–265.

[10] I.M. Wekesa, D. Jaganyi, Dalton Trans. 43 (2014) 2549–2558.

[11] a) D. Jaganyi, A. Hofmann, R. van Eldik, Angew. Chem. Int. Ed. 40 (2001) 1680–1683;
b) A. Hofmann, D. Jaganyi, O.Q. Munro, G. Liehr, R. van Eldik, Inorg. Chem. 42 (2003) 1688–1700.

[12] A. Hofmann, L. Dahlenburg, R. van Eldik, Inorg. Chem. 42 (2003) 6528–6538.

[13] a) D. Jaganyi, K.L.D. Boer, J. Gertenbach, J. Perils, Int. J. Chem. Kinet. 40 (2008) 808–818;
b) D. Jaganyi, D. Reddy, J. Gertenbach, A. Hofmann, R. van Eldik, Dalton Trans. (2004) 299–304.

[14] a) P. Ongoma, D. Jaganyi, Dalton Trans. 41 (2012) 10724–10730;
b) G. Kinunda, D. Jaganyi, Transit. Met. Chem. 39 (2014) 451–459;
c) B.B. Khusi, A. Mambanda, D. Jaganyi, J. Coord. Chem. 69 (2016) 2121–2135.

[15] a)B. Petrović, Ž.D. Bugarčić, A. Dees, I. Ivanović-Burmazović, F. W. Heinemann, R. Puchta, S. N. Steinmann, C. Corminboeuf, R. Van Eldik, *Inorganic Chemistry* **2012**, *51*, 1516-1529.b) A. Mijatović, J. Bogojeski, B. Petrović, Ž.D. Bugarčić, Inorg. Chim. Acta 383 (2012) 300–304.

[16] a) E. Breet, R. Van Eldik, Inorg. Chem. 23 (1984) 1865–1869;
b) M. Kotowski, R. Van Eldik, Inorg. Chem. 23 (1984) 3310–3312;
c) M. Kotowski, R. Van Eldik, Inorg. Chem. 25 (1986) 3896–3899;
d) J. Pienaar, M. Kotowski, R. Van Eldik, Inorg. Chem. 28 (1989) 373–375;
e) J. Berger, M. Kotowski, R. Van Eldik, U. Frey, L. Helm, A. Merbach, Inorg. Chem. 28 (1989) 3759–3765.

[17] a) A. Mambanda, D. Jaganyi, in *Advances in Inorganic Chemistry, Vol. 70*, Elsevier, **2017**, pp. 243-276; b) I. M. Wekesa, D. Jaganyi, *Journal of Coordination Chemistry* **2016**, *69*, 389-403; c) I. M. Wekesa, PhD Thesis thesis, University of KwaZulu-Natal, South Africa (South Africa), **2014**; d) I. M. Wekesa, D. Jaganyi, *Transition Metal Chemistry* **2021**, *46*, 363-371.

[18] M.L. Tobe, J. Burgess, Inorganic reaction mechanisms, Longman, London, 1999, pp. 30–112.

[19] a) S.G. Murray, F.R. Hartley, Chem. Rev. 81 (1981) 365–414;
b) J. Reedijk, Chem. Rev. 99 (1999) 2499–2510.

[20] a) W.C. Schiessl, N.K. Summa, C.F. Weber, S. Gubo, C. Dücker-Benfer, R. Puchta, N.J. van Eikema Hommes, R. van Eldik, Z. Anorg. Allg. Chem. 631 (2005) 2812–2819;
b) M.T. Ashby, Comments Inorg. Chem. 10 (1990) 297–313.

[21] W.O. Siegl, J. Org. Chem. 42 (1977) 1872–1878.

[22] K. Hanson, N. Patel, M.T. Whited, P.I. Djurovich, M.E. Thompson, Org. Lett. 13 (2011) 1598–1601.

[23] O.V. Dolomanov, L.J. Bourhis, R.J. Gildea, J.A. Howard, H. Puschmann, J. Appl. Cryst. 42 (2009) 339–341.

[24] G.M. Sheldrick, Acta Crystallogr. A 64 (2008) 112–122.

[25] G.M. Sheldrick, Acta Crystallogr. Section C: Struct. Chem. 71 (2015) 3–8.

[26] M. Frisch, G. Trucks, H. Schlegel, G. Scuseria, M. Robb, J. Cheeseman, G. Scalmani, V. Barone, B. Mennucci, G. Petersson, Gaussian, Inc., Wallingford CT, **2009**.

[27] a) A.D. Becke, J. Chem. Phys. 98 (1993) 5648–5652;
b) C. Lee, W. Yang, R.G. Parr, Phys. Rev. B 37 (1988) 785–789.

[28] P.J. Hay, W.R. Wadt, J. Chem. Phys. 82 (1985) 299–310.

[29] a) V. Barone, M. Cossi, Chem. A Eur. J. 102 (1998) 1995–2001;
b) M. Cossi, N. Rega, G. Scalmani, V. Barone, J. Comput. Chem. 24 (2003) 669–681.

[30] a) T. Appleton, J. Hall, S. Ralph, C. Thompson, Inorg. Chem. 23 (1984) 3521–3525;
b) D. Reddy, K.J. Akerman, M.P. Akerman, D. Jaganyi, Transit. Met. Chem. 36 (2011) 593–602.

[31] a) R. Bellam, D. Jaganyi, R.S. Robinson, ACS Omega 7 (2022) 26226–26245;
b) G. Vidyavathi, B.V. Kumar, A.V. Raghu, T. Aravinda, U. Hani, H.A. Murthy, A. Shridhar, J. Mol. Struct. 1249 (2022), 131656;
c) S. Gurusamy, K. Krishnaveni, M. Sankarganesh, R.N. Asha, A. Mathavan, J. Mol. Liq. 345 (2022), 117045;
d) R.O. Omondi, A.O. Fadaka, A.A. Fatokun, D. Jaganyi, S.O. Ojwach, J. Biol. Inorg. Chem. 27 (2022) 653–664;
e) R.O. Omondi, N.R. Sibuyi, A.O. Fadaka, M. Meyer, D. Jaganyi, S.O. Ojwach, Dalton Trans. 50 (2021) 8127–8143.

[32] O. Trott, A.J. Olson, J. Comput. Chem. 31 (2010) 455–461.

[33] M. Bröring, C. Kleeberg, Inorg. Chim. Acta 362 (2009) 1065–1070.

[34] M. Bröring, C. Kleeberg, E. Cónsul Tejero, Eur. J. Inorg. Chem. (2007, 2007,) 3208–3216.

[35] S.A. Willison, H. Jude, R.M. Antonelli, J.M. Rennekamp, N.A. Eckert, J.A. Krause Bauer, W.B. Connick, Inorg. Chem. 43 (2004) 2548–2555.

[36] E. Seifert, J. Chem. Informat. Modell. 54 (2014) 1552.

[37] H. Eyring, J. Chem. Phys. 3 (1935) 107–115.

[38] a) A. Mambanda, D. Jaganyi, S. Hochreuther, R. van Eldik, *Dalton Transactions* **2010**, *39*, 3595-3608; b) P. A. Wangoli, G. Kinunda, *New J. Chem.* **2018**, *42*, 214-227; c) A. Shaira, PhD Thesis thesis, University of KwaZulu-Natal, South Africa (South Africa), **2013**.

[39] a) P.O. Ongoma, D. Jaganyi, Dalton Trans. 42 (2013) 2724–2734;
b) P.W. Asman, Inorg. Chim. Acta 469 (2018) 341–352;
c) W.P. Asman, D. Jaganyi, Int. J. Chem. Kinet. 49 (2017) 545–561;
d) P.W. Asman, J. Coord. Chem. (2017) 1371702–1371722.

[40] a) D.O. Onunga, D. Jaganyi, A. Mambanda, J. Coord. Chem. 72 (2019) 499–515;
b) A. Shaira, D. Reddy, D. Jaganyi, Dalton Trans. 42 (2013) 8426–8436.

[41] M.E. Oehlsen, A. Hegmans, Y. Qu, N. Farrell, J. Biol. Inorg. Chem. 10 (2005) 433–442.

[42] a) H. Ertürk, R. Puchta, R. van Eldik, Eur. J. Inorg. Chem. 2009 (2009) 1331–1338;
b) A. Mambanda, D. Jaganyi, Dalton Trans. 40 (2011) 79–91.

[43] a) D. Jaganyi, F. Tiba, Transit. Met. Chem. 28 (2003) 803–807;
b) D. Reddy, D. Jaganyi, Transit. Met. Chem. 31 (2006) 792–800.

[44] a) F. Basolo, R.G. Pearson, Mechanisms in Inorganic Reactions, 2nd ed., Wiley, New York, 1967;
b) J.D. Atwood, Inorganic and organometallic reaction mechanisms, 2nd ed., Wiley-VCH Publishers, New York, 1997;
c) R. Van Eldik, T. Asano, W. Le Noble, Chem. Rev. 89 (1989) 549–688.

[45] P. Sathyadevi, P. Krishnamoorthy, R.R. Butorac, A.H. Cowley, N.S. Bhuvanesh, N. Dharmaraj, Dalton Trans. 40 (2011) 9690–9702.

[46] a) M. Feizi-Dehnayebi, E. Dehghanian, H. Mansouri-Torshizi, J. Mol. Liq. 344 (2021), 117853;
b) B. Saygıdeğer Demir, S. İnce, M.K. Yilmaz, A. Sezan, E. Derinöz, T. Taskin-Tok, Y. Saygideger, Pharmaceutics 14 (2022) 2409.

[47] J.-B. LePecq, C. Paoletti, J. Mol. Biol. 27 (1967) 87–106.

[48] P. Kumar, S. Dasari, A.K. Patra, Eur. J. Med. Chem. 136 (2017) 52–62.

[49] I. Mitra, S. Mukherjee, B. Misini, P. Das, S. Dasgupta, W. Linert, S.C. Moi, New J. Chem. 42 (2018) 2574–2589.

[50] A. Jahanban-Esfahlan, L. Roufegarinejad, R. Jahanban-Esfahlan, M. Tabibiazar, R. Amarowicz, Talanta 207 (2020), 120317.

[51] C. Kakoulidou, C.T. Chasapis, A.G. Hatzidimitriou, K.C. Fylaktakidou, G. Psomas, Dalton Trans. 51 (2022) 16688–16705.

[52] S.A. Patra, A. Banerjee, G. Sahu, M. Mohanty, S. Lima, D. Mohapatra, H. Görls, W. Plass, R. Dinda, J. Inorg. Biochem. 233 (2022), 111852.

[53] S. Mandal, S.K. Tarai, P. Patra, P. Nandi, S. Sing, B. Rajak, S.C. Moi, Langmuir 38 (2022) 13613–13625.

[54] P. Kumar, P. Singh, S. Saren, S. Pakira, S. Sivakumar, A.K. Patra, Dalton Trans. 50 (2021) 8196–8217.

[55] Z.-J. Cheng, H.-M. Zhao, Q.-Y. Xu, R. Liu, J. Pharm. Anal. 3 (2013) 257–269.